

# Hybrid RANS/LES Calculations in SU2

Eduardo S. Molina,\* Cleber Spode† Roberto Gil A. da Silva‡

*ITA - Instituto Tecnológico de Aeronáutica, São José dos Campos, Brasil*

David E. Manosalvas-Kjono§ Savvy Nimmagadda§ Thomas D. Economon¶ Juan J. Alonso||

*Stanford University, Stanford, CA 94305, U.S.A.*

Marcello Righi\*\*

*Zurich University of Applied Sciences, Winterthur, Switzerland*

This paper presents a detailed overview of hybrid RANS/LES methods as implemented within the open-source Stanford University Unstructured (SU2) software package. We focus on the extensions of the existing RANS framework based upon the Spalart-Allmaras turbulence model that are necessary to apply the Delayed Detached-Eddy Simulation (DDES) technique. Particular emphasis is placed upon the low dissipation and low Mach number convective schemes required to maintain accuracy within the context of performing DDES in a second-order, finite volume, unstructured flow solver. We conclude with a suite of test cases across different regimes to demonstrate our DDES capability on both academic and industrial-grade applications.

## I. Introduction

The hybrid RANS-LES turbulence modeling technique, often called DES (Detached Eddy Simulation) or DDES (Delayed detached Eddy Simulation) referring to the most notable implementations,<sup>1,2</sup> applies the RANS and the LES approach in different regions of the computational domain depending on the available spatial and temporal resolution. The partitioning may be assigned *a-priori*<sup>3</sup> or automatically by the solver on the basis of the local RANS and LES turbulent length-scales.

This technique targets high Reynolds-number flow cases, characterized by large turbulent scales, exploiting the better physical consistence of LES to resolve the complex areas of the flow, and the inexpensive nature of the RANS approach inside the boundary-layer.

The potential industrial “value” of the hybrid RANS-LES modeling is significant: its applications include the analysis of space vehicles engines, aircraft’s landing configurations, shock separated flow at the boundaries of the flight envelope, off-design conditions of turbines and compressors, combustion chambers, and latest generation wind turbine’s blades dynamics.

Arguably, this technique has not yet reached a maturity level which would allow its systematic use in industrial environment; two main issues are still actively investigated: the physical consistence of the interface between RANS and LES also known as “gray area” and prevention of the flow re-laminarization following a too early switch to LES, or “RANS shielding”. The interested reader is referred to the proceedings of the bi-annual HRLM symposium<sup>4-6</sup> and references therein.

An extension of SU2 to include hybrid turbulence models is of double relevance: firstly, it would improve the analysis of flow cases and configurations characterized by separated flow and, secondly, it would provide a convenient open-source framework for further development of these models. As an open-source package,

\*Ph.D. Candidate, Department of Aeronautics & Mechanics. E-mail:molinaedu85@gmail.com

†Ph.D. Candidate, Department of Aeronautics & Mechanics.

‡Professor, Department of Aeronautics & Mechanics.

§Ph.D. Candidate, Department of Aeronautics & Astronautics, AIAA Student Member.

¶Postdoctoral Scholar, Department of Aeronautics & Astronautics, AIAA Senior Member.

||Professor, Department of Aeronautics & Astronautics, AIAA Associate Fellow.

\*\*Professor, School of Engineering, AIAA Member

SU2 is uniquely positioned to serve as an example to computational scientists around the world. Its open-source nature allows for rapid and effective technology transfer to the community, which increases the pace of research and innovation in the computational sciences and engineering.

In order to demonstrate the initial implementation of hybrid RANS/LES models in SU2, the following benchmark test cases have been chosen as a representative set of the broader range of scale-resolving applications for which SU2 could be used:

- Spatial shear layer.
- Zero gradient flat plate.
- Backward facing step.
- NACA0021 airfoil in deep stall.

## II. Methodology

We are concerned with compressible, turbulent fluid flows governed by the Navier-Stokes equations, which can be expressed in differential form as

$$\left\{ \begin{array}{ll} R(U) = \frac{\partial U}{\partial t} + \nabla \cdot \vec{F}_{ale}^c - \nabla \cdot (\mu_{tot}^1 \vec{F}^{v1} + \mu_{tot}^2 \vec{F}^{v2}) - Q = 0, & \text{in } \Omega, \quad t > 0 \\ \vec{v} = \vec{u}_\Omega, & \text{on } S, \\ \partial_n T = 0, & \text{on } S, \\ (W)_+ = W_\infty, & \text{on } \Gamma_\infty, \end{array} \right. \quad (1)$$

where the conservative variables are expressed by  $U = \{\rho, \rho\vec{v}, \rho E\}^T$ . The second line of Eq.1 represents the no-slip condition at the wall, the third line represents an adiabatic condition at the wall and the final line represents a characteristic-based boundary condition at the far-field.  $W$  represents the characteristic variables.

For problems on fixed grids,  $\vec{u}_\Omega = 0$ , Eq.1 reduces to a purely Eulerian formulation. The convective fluxes, viscous fluxes and source term are

$$\vec{F}_{ale}^c = \begin{Bmatrix} \rho(\vec{v} - \vec{u}_\Omega) \\ \rho\vec{v} \otimes (\vec{v} - \vec{u}_\Omega) + \bar{I}p \\ \rho E(\vec{v} - \vec{u}_\Omega) + p\vec{v} \end{Bmatrix}, \vec{F}^{v1} = \begin{Bmatrix} \cdot \\ \bar{\tau} \\ \bar{\tau} \cdot \vec{v} \end{Bmatrix}, \vec{F}^{v2} = \begin{Bmatrix} \cdot \\ \cdot \\ c_p \nabla T \end{Bmatrix}, \mathcal{Q} = \begin{Bmatrix} q_\rho \\ \vec{q}_{\rho\vec{v}} \\ q_{\rho E} \end{Bmatrix}. \quad (2)$$

$\rho$  is the fluid density,  $\vec{v} = \{v_1, v_2, v_3\}^T \in \mathbb{R}^3$  is the flow speed in Cartesian system of reference,  $\vec{u}_\Omega$  is the velocity of a moving domain,  $E$  is the total energy per unit mass,  $p$  is the static pressure,  $c_p$  is the specific heat at constant pressure,  $T$  is the temperature and the viscous stress can be expressed in a vector notation as

$$\bar{\tau} = \nabla \vec{v} + \nabla \vec{v}^T - \frac{2}{3} \bar{I} (\nabla \cdot \vec{v}). \quad (3)$$

Assuming a calorically perfect gas with a ratio of specific heats,  $\gamma$ , and gas constant,  $R$ , the pressure is determined from

$$p = (\gamma - 1) \rho \left[ E - \frac{1}{2} (\vec{v} \cdot \vec{v}) \right], \quad (4)$$

the temperature is defined as

$$T = \frac{P}{\rho R} \quad (5)$$

and

$$c_p = \frac{\gamma R}{(\gamma - 1)}. \quad (6)$$

For unsteady turbulent flows, we are interested in obtaining the solutions of the unsteady Reynolds-Average Navier-Stokes (URANS), which will require the inclusion of a suitable turbulence model. In accord

with the standard approach to turbulence based upon the Boussinesq hypothesis,<sup>7</sup> which states that the effect of turbulence can be represented as an increased viscosity, the total viscosity can be divided into a laminar  $\mu_{dyn}$  and turbulent  $\mu_{tur}$  component. In order to close the system of equations, the dynamic viscosity is assumed to satisfy Sutherland's law:<sup>8</sup>

$$\mu_{dyn} = 1.716 * 10^{-5} \left[ \frac{T}{273.15} \right]^{\frac{3}{2}} \left[ \frac{273.15 + 110.4}{T + 110.4} \right], \quad (7)$$

and the turbulent viscosity ( $\mu_{tur}$ ) is modeled, which allows for the computation of the total viscosity

$$\mu_{tot}^1 = \mu_{dyn} + \mu_{tur}, \quad \mu_{tot}^2 = \frac{\mu_{dyn}}{Pr_d} + \frac{\mu_{tur}}{Pr_t}, \quad (8)$$

where  $Pr_d$  and  $Pr_t$  are the dynamic and turbulent Prandtl numbers, respectively and  $\mu_{tot}^2$  represents the effective thermal conductivity.

The turbulent viscosity is obtained from a suitable turbulence model that depends on the flow state and a set of new variables,  $\hat{\nu}$ , i.e.,  $\mu_{tur} = \mu_{tur}(U, \hat{\nu})$ . Here, the scalar variable  $\hat{\nu}$  is obtained from a one-equation turbulence model. The Spalart-Allmaras (SA)<sup>9</sup> model is one of the most common and widely used turbulence models for the analysis and design of engineering/aerospace applications in turbulent flows.

### A. Spalart-Allmaras (SA) Model

The adopted turbulence model in this study is the Spalart-Allmaras model.<sup>9</sup> Here, the turbulent viscosity is computed as

$$\mu_{tur} = \rho \hat{\nu} f_{v1}, \quad f_{v1} = \frac{\chi^3}{\chi^3 + c_{v1}^3}, \quad \chi = \frac{\hat{\nu}}{\nu}, \quad \nu = \frac{\mu_{dyn}}{\rho}. \quad (9)$$

The new variable  $\hat{\nu}$  is obtained by solving the transport equation, Eq.10, in conjunction with the mean flow equations.

$$\begin{cases} R_{\hat{\nu}}(U, \hat{\nu}) = \frac{\partial \hat{\nu}}{\partial t} + \nabla \cdot \vec{F}^c - \nabla \cdot \vec{F}^v - Q = 0, & \text{in } \Omega, \quad t > 0 \\ \hat{\nu} = 0, & \text{on } S, \\ \hat{\nu} = \sigma_{\infty} \hat{\nu}, & \text{on } \Gamma_{\infty}, \end{cases} \quad (10)$$

where the convective, viscous and source terms are given by

$$\vec{F}^c = \vec{v} \hat{\nu}, \quad \vec{F}^v = -\frac{\nu + \hat{\nu}}{\sigma} \nabla \hat{\nu}, \quad Q = c_{b1} \hat{S} \hat{\nu} + \frac{c_{b2}}{\sigma} |\nabla \hat{\nu}|^2 - c_{w1} f_w \left( \frac{\hat{\nu}}{d} \right)^2, \quad (11)$$

where  $d$  is the distance to the nearest wall. The production term  $\hat{S}$  and functions  $f_{v1}$ ,  $f_{v2}$  and  $f_w$  are given by:

$$\hat{S} = |\vec{\omega}| + \frac{\hat{\nu}}{k^2 d_S^2} f_{v2}, \quad f_{v1} = \frac{\chi^3}{\chi^3 + c_{v1}^3}, \quad f_{v2} = 1 - \frac{\chi}{1 + \chi f_{v1}}, \quad f_w = g \left[ \frac{1 + C_{w3}^6}{g^6 + C_{w3}^6} \right]^{1/6}, \quad (12)$$

where  $g = r + c_{w2}(r^6 - r)$  and  $r = \frac{\hat{\nu}}{\hat{S} k^2 d_S^2}$ . Finally, the set of closure constants for the model is given by

$$\sigma = \frac{2}{3}, c_{b1} = 0.1355, c_{b2} = 0.622, \kappa = 0.41, c_{w1} = \frac{c_{b1}}{\kappa^2} + \frac{1 + c_{b2}}{\sigma}, c_{w2} = 0.3, c_{w3} = 2, c_{v1} = 7.1 \quad (13)$$

In Eq.10,  $\hat{\nu}$  is set to zero on viscous walls which means that there are no turbulent eddies near the wall. At the far-field, a fraction of the laminar viscosity is imposed.

## III. Hybrid RANS-LES Models

A common view of turbulent flows is that turbulence consists of a range of scales, from larger scales often determined by the geometry to the smaller scales determined by fluid viscosity. This broad range of scales lead to the conflicting choice of modeling Vs. resolving the turbulent scales.

The Navier-Stokes equations are a remarkably exact description of turbulence. The Direct Numerical Simulation (DNS) solves all the turbulent scales at the limit of a sufficiently fine grid with sufficiently small time step, requiring very accurate numerical methods and boundary conditions. However, at high Reynolds number, typical of industrial applications, the grid size increases proportionally with the range of scales that needed to be resolved, making this option extremely computationally expensive.

As an alternative, with Large Eddy Simulation (LES), just roughly 10% of the turbulence is modeled, which is relative to the smaller scales.<sup>10</sup> The remaining larger scales are resolved as in DNS. Unfortunately, wall-bounded flows, at high Reynolds number, continues to be computationally unaffordable due to the grid size needed to resolve turbulent scales inside the boundary-layer, even with the introduction of wall models.<sup>11</sup>

On the other hand, RANS methods capture only the mean flow (or sometimes only the largest scales) while modeling the effect of all the fluctuations. In addition, RANS models are calibrated for attached flows such as flow over a flat plate, and hence provide results with engineering accuracy and manageable uncertainties for such cases.

For this reason, it seems natural to attempt a combination of both turbulence modeling approaches, use RANS in regions where it is reliable and efficient,<sup>12</sup> while using LES elsewhere. Due to the low turbulence model influence and reasonable cost, hybrid methods are attractive for industrial applications.

### A. Detached-Eddy Simulation

One of the most popular Hybrid RANS/LES methods is Detached Eddy Simulation (DES), which was first proposed by Spalart et al.<sup>1</sup> The original DES formulation is based on the SA turbulence model<sup>9</sup> and it introduced a modified length scale definition

$$\tilde{d} = \min(d, C_{DES}\Delta), \quad (14)$$

$$\Delta = \max(\Delta_x, \Delta_y, \Delta_z), \quad (15)$$

where  $d$  is the distance to the wall,  $\Delta$  is the local maximum grid spacing and  $C_{DES} = 0.65$  is the model constant calibrated by means of isotropic turbulence.<sup>11</sup>

The last term in Eq.11 represents a destruction term for  $\tilde{\nu}$  depending on the wall distance  $d$ . In the near-wall region, where  $d < C_{DES}\Delta$ , the model employed is the original RANS model. Away from the wall, where  $d > C_{DES}\Delta$ , the model turns into a similar Smagorinsky LES sub-grid scale (SGS) model. A reduced length scale increases the destruction term and hence yields a reduced eddy viscosity.

### B. Delayed Detached-Eddy Simulation

Typical DES grids normally have the grid spacing in the parallel direction to the surface larger than the boundary layer thickness. In some cases, however, surface grids may become excessively refined to represent some feature of the geometry or the proper resolution of a shock wave, for example. In this situation, the original DES length scale can become smaller than the boundary layer thickness, thus, leading to a condition of “ambiguous grid density” for the original DES and an erroneous activation of the LES mode inside the attached boundary-layer.

As a consequence, the effective length scale is abruptly reduced, lowering the eddy viscosity and the modeled Reynolds stresses without the generation of a proper LES content. This issue is known as “modeled-stress depletion” (MSD). As reported by Menter and Kuntz,<sup>13</sup> MSD may potentially reduce the skin-friction and in some severe cases can cause grid-induced separation.<sup>14</sup>

Spalart et al<sup>2</sup> proposed a general solution to MSD that detects and “shields” attached boundary-layers delaying the activation of the LES mode even on ambiguous grids, for this reason, it was named Delayed Detached-Eddy Simulation (DDES). This is achieved by re-defining the length scale,  $\tilde{d}$  as:

$$\tilde{d} = d - f_d \max(0, d - C_{DES}\Delta), \quad (16)$$

where  $f_d$  is a coefficient that can be estimated by the following equations:<sup>2</sup>

$$f_d = 1 - \tanh((8r_d)^3), \quad (17)$$

$$r_d = \frac{\tilde{\nu} + \nu}{\sqrt{U_{i,j}U_{i,j}k^2d^2}}, \quad (18)$$

where  $U_{i,j}$  is the velocity gradient,  $k$  is Karman constant and  $d$  is the distance to the nearest wall.

The  $r_d$  parameter is used to design the delaying function  $f_d$ , which is capable of distinguishing RANS and LES regions,  $f_d$  is equal to zero in RANS regions and to one in all other zones.

In addition to wall distance and grid size dependence, the DDES formulation is influenced by the local flow physics avoiding the undesirable switching to LES when using ambiguous grids.

Since its original DES conception, and later extensions and improvements (delayed DES (DDES)<sup>2</sup> and improved DDES (IDDES),<sup>15</sup> has become a powerful computational tool for complex aerodynamic and aeroacoustic problems. However, some DES-related issues still remain unresolved.

This, first of all, concerns the so-called “Grey Area” issue. In the free shear layers and jet flows, this issue manifests itself in a significant delay of the natural Kelvin-Helmholtz instability and “secondary transition” to turbulence. This delay prevents a plausible representation of turbulence in the initial regions of the shear layers. To overcome the slow transition from RANS to LES in shear-layer flows, different recently-proposed modification of the sub-grid length scale (SGS) were converted to handle unstructured grids and implemented in SU2: these include both Vorticity-based SGS<sup>16</sup> and Shear-Layer Adapted SGS.<sup>17</sup>

### 1. Vorticity-Based SGS

The Zonal Detached-Eddy Simulation (ZDES) was originally developed by Deck.<sup>18</sup> This formulation was designed for structured multi-block solvers where, the user defines *a-priori* both RANS and LES regions. The ZDES approach is not possible herein since, SU2 is based on an unstructured finite volume method.

However, Deck<sup>16</sup> proposed a new definition of the sub-grid length scale for ZDES based on the vorticity alignment to overcome the slow LES content development in mixing layers. This sub-grid can be extended to unstructured solvers as

$$\Delta_\omega = \sqrt{n_x^2 \Delta_y \Delta_z + n_y^2 \Delta_x \Delta_z + n_z^2 \Delta_x \Delta_y}, \quad (19)$$

where  $n_x$ ,  $n_y$  and  $n_z$  are the unit vector aligned with the vorticity vector.

### 2. Shear-layer Adapted SGS

Shur et al.<sup>17</sup> argued that the slow transition between RANS/LES has its origin associated with peculiarities of the grids typically used in DES. In particular, in order to capture the initial region, these grids are refined across the shear layers and, typically to a lesser extent, in the streamwise direction, but are relatively coarse in the spanwise direction. This creates strongly anisotropic grid cells which are very different from the nearly isotropic cells assumed when pure LES or LES mode within DES are applied.

Based on this idea, Shur et al.<sup>17</sup> proposed a new sub-grid length scale, namely Shear-Layer Adapted (SLA), that sensitizes the DES cell-size measure to strongly anisotropic cells in early shear layers.

$$\tilde{\Delta}_\omega = \frac{1}{\sqrt{3}} \max |(I_n - I_m)|, \quad (20)$$

where  $I_n = n_\omega \times r_n$  and  $n_\omega$  is the unit vector aligned with the vorticity vector and  $r_n$  is the cell center vector.

$$\Delta_{SLA} = \tilde{\Delta}_\omega F_{KH}(< VTM >), \quad (21)$$

where  $F_{KH}$  is a piecewise-linear function defined as

$$F_{KH}(< VTM >) = \max(F_{KH}^{min}, \min(F_{KH}^{max}, F_{KH}^{min} + \frac{F_{KH}^{max} - F_{KH}^{min}}{a_2 - a_1} (< VTM > - a_1))). \quad (22)$$

Here  $F_{KH}^{max} = 1.0$ ,  $F_{KH}^{min} = 0.1$ ,  $a_1 = 0.15$  and  $a_2 = 0.3$ .  $VTM$  is the Vortex Tilting Measure defined as

$$VTM = \frac{\sqrt{6}|(\hat{S} \cdot \omega) \times \omega|}{\omega^2 \sqrt{3tr(\hat{S}^2) - [tr(\hat{S})]^2}} \max 1, (\nu^*/\nu_t), \quad \nu^* = 0.2\nu, \quad (23)$$

where  $\hat{S}$  is the strain tensor and  $\omega$  is the vorticity.

## IV. Numerical Implementation

In this section, we first present a high level overview of the SU2 package as background before discussing implementation and considerations pertinent to an accurate hybrid RANS/LES capability in an unstructured flow solver. In particular, low-Mach and low-dissipation second-order convective schemes appropriate for hybrid RANS/LES calculations in the present regime will be discussed.

### A. Overview of the SU2 Flow Solver

The SU2 software suite<sup>19–21</sup> is an open-source collection of software tools written in C++ and Python for performing multi-physics simulation and design. It is built specifically for the analysis of partial differential equations (PDEs) and PDE-constrained optimization problems on unstructured meshes with state-of-the-art numerical methods, and it is particularly well suited for aerodynamic shape design. The initial applications of the suite were mostly in aerodynamics, but through the initiative of users and developers around the world, SU2 is now being used for a wide variety of problems beyond aeronautics, including automotive, naval, and renewable energy applications, to name a few.

#### 1. Spatial Integration

In SU2, both finite volume and finite element discretizations are available, but in this work, we focus on second-order finite volume schemes. The finite volume method (FVM)<sup>22–29</sup> is applied on the unstructured meshes in SU2 using a standard edge-based data structure on a dual grid with control volumes constructed using a median-dual, vertex-based scheme. Median-dual control volumes are formed by connecting the centroids, face, and edge midpoints of all primal cells sharing the particular vertex.

After integrating the governing equations over a control volume and applying the divergence theorem, one obtains the semi-discretized, integral form:

$$\begin{aligned} 0 &= \int_{\Omega_i} \frac{\partial U}{\partial t} d\Omega + \sum_{j \in \mathcal{N}(i)} (\tilde{F}_{ij}^c + \tilde{F}_{ij}^v) \Delta S_{ij} - Q |\Omega_i| \\ &= \int_{\Omega_i} \frac{\partial U}{\partial t} d\Omega + R_i(U), \end{aligned} \quad (24)$$

where  $R_i(U)$  is the numerical residual that represents the integration of all spatial terms for the control volume surrounding vertex  $i$ .  $\tilde{F}_{ij}^c$  and  $\tilde{F}_{ij}^v$  are the numerical approximations of the convective and viscous fluxes projected along an edge, respectively, and  $Q$  is the source term.  $\Delta S_{ij}$  is the area of the face associated with the edge  $ij$ ,  $|\Omega_i|$  is the volume of the dual control volume, and  $\mathcal{N}(i)$  is the set of neighboring vertices to vertex  $i$ .

The convective and viscous fluxes are evaluated at the midpoint of an edge. The convective fluxes can be discretized using centered or upwind schemes in SU2. Typical choices are the Jameson-Schmidt-Turkel (JST) scheme,<sup>30</sup> or the approximate Riemann solver of Roe,<sup>31</sup> which will be discussed in detail below. Second-order reconstruction for upwind methods is achieved via the MUSCL approach.<sup>32</sup> Slope limiting is applied to preserve monotonicity in the solution by limiting the gradients during higher-order reconstruction, and the Venkatakrishnan<sup>33</sup> limiter is a common choice for this. The convective term for the scalar variable in the S-A turbulence model is discretized using a first-order or second-order fully upwind scheme.

In order to evaluate the viscous fluxes with a finite volume method for both the mean flow and turbulence model, flow quantities and their first derivatives are required at the faces of the dual control volumes. The spatial gradients of the flow variables are calculated in a pre-processing step at all vertices using Green-Gauss or Least-Squares approach<sup>34</sup> and then averaged to obtain these gradients at the cell faces when computing viscous fluxes along the edges. Source terms are approximated at each vertex using piece-wise constant reconstruction within each of the dual control volumes.

In practice, the numerical residual  $R_i(U)$  at each vertex from Eqn. 24 is evaluated with each nonlinear iteration using a sequence of loops over the edges and vertices. This series of steps results in a value of  $R_i(U)$  at each vertex at a particular instance in time, which is then be substituted into Eqn. 24 and integrated in time to arrive at either a steady state or a time-accurate solution for the state vector  $U$ .

## 2. Time Integration

We now consider the techniques for time-marching the coupled system of ordinary differential equations for the flow problem presented in Eqn. 24, which can be rewritten as

$$\frac{d}{dt} (|\Omega_i| U_i) + R_i(U) = 0, \quad (25)$$

where  $|\Omega_i| = \int_{\Omega_i(t)} d\Omega$ . Here, we are assuming that there is no dynamic mesh motion, i.e., change in the control volumes, during time integration. By discretizing the time derivative term, one obtains a fully-discrete finite volume form of the governing equations.

For particularly stiff problems, implicit methods can be used to improve convergence due to their increased numerical stability. Here, we use the backward Euler scheme, where the residual is evaluated using the solution state at the new time level  $U^{n+1}$ . Applying this to Eqn. (25), one has

$$|\Omega_i| \frac{\Delta U_i}{\Delta t_i} = -R_i(U^{n+1}), \quad (26)$$

where time level  $n$  corresponds to the known solution in its current state, while time level  $n+1$  represents the new solution state that is being sought after advancing one time step  $\Delta t$  where  $\Delta t = t^{n+1} - t^n$  and  $\Delta U_i = U_i^{n+1} - U_i^n$ . However, the residuals at time level  $n+1$  are now a function of the unknown solution state  $U^{n+1}$  and can not be directly computed. Therefore, a first-order linearization about time level  $n$  is performed:

$$R_i(U^{n+1}) = R_i(U^n) + \sum_{j \in \mathcal{N}(i)} \frac{\partial R_i(U^n)}{\partial U_j} \Delta U_j^n + \mathcal{O}(\Delta t^2). \quad (27)$$

Introducing Eqn. (27) into Eqn. (26), we find that the following linear system should be solved to find the solution update ( $\Delta U_i^n$ ):

$$\left( \frac{|\Omega_i|}{\Delta t_i^n} \delta_{ij} + \frac{\partial R_i(U^n)}{\partial U_j} \right) \cdot \Delta U_j^n = -R_i(U^n), \quad (28)$$

where if a flux  $\tilde{F}_{ij}$  has a stencil of points  $\{i, j\}$ , then contributions are made to the Jacobian at four points, or

$$\frac{\partial R}{\partial U} := \frac{\partial R}{\partial U} + \begin{bmatrix} \ddots & & & \\ & \frac{\partial \tilde{F}_{ij}}{\partial U_i} & \cdots & \frac{\partial \tilde{F}_{ij}}{\partial U_j} \\ & \vdots & \ddots & \vdots \\ & -\frac{\partial \tilde{F}_{ij}}{\partial U_i} & \cdots & -\frac{\partial \tilde{F}_{ij}}{\partial U_j} \\ & & & \ddots \end{bmatrix}. \quad (29)$$

Implicit methods enable the use of higher CFL conditions than with explicit methods, which translate to the specific values of  $\Delta t_i$  that are used to relax the problem. For steady problems, a constant time step for all cells is not required, and a local time-stepping technique can be used to accelerate convergence to a steady state. Allowable local time-step values can be calculated from an estimation of the convective and viscous spectral radii at every vertex in the mesh.<sup>35</sup> The resulting linear systems are typically solved using a preconditioned Generalized Minimal Residual (GMRES) method.<sup>36</sup>

A dual time-stepping strategy<sup>37,38</sup> has been implemented to achieve high-order accuracy in time. In this method, the unsteady problem is transformed into a series of steady problems at each physical time step that can then be solved using all of the well-known convergence acceleration techniques for steady problems.

To apply the dual time-stepping strategy, a fictitious or pseudo time derivative is introduced in front of the original governing equations to give

$$\frac{\partial U}{\partial \tau} + R_i^*(U) = 0, \quad (30)$$

where, for a second-order backward difference in time,

$$R_i^*(U) = \frac{3}{2\Delta t} U_i + \frac{1}{|\Omega_i|^{n+1}} \left( R_i(U) - \frac{2}{\Delta t} |\Omega_i|^n U_i^n + \frac{1}{2\Delta t} |\Omega_i|^{n-1} U_i^{n-1} \right), \quad (31)$$

where  $\Delta t$  is a chosen physical time step and we have also assumed that the equations will be solved in a fully implicit manner by expressing the spatial residual in terms of the solution at time level  $n + 1$ .

Converging the steady problem defined by Eqn. 30 in pseudo time at each physical time step (including any convergence acceleration techniques for steady problems) results in the modified residual being equal to zero, or  $R_i^*(U) = 0$ , which is equivalent to finding the state  $U = U^{n+1}$ .

## B. Upwind Roe Flux-Difference Splitting Scheme

This section presents the flux-difference splitting scheme of Roe<sup>31</sup> which is one of the most common numerical scheme used for computing convective fluxes.

The Roe scheme is an approximate Riemann solver, it evaluates the convective fluxes from flow quantities reconstructed separately on both sides of the face of the dual control volume from values at the surrounding nodes:

$$\tilde{F}_{ij}^c = \left( \frac{\vec{F}_i^c + \vec{F}_j^c}{2} \right) \cdot \vec{n}_{ij} - \frac{1}{2} P |\Lambda| P^{-1} (U_i - U_j) - (\vec{u}_{\Omega_{ij}} \cdot \vec{n}_{ij}) \left( \frac{U_i + U_j}{2} \right), \quad (32)$$

where  $\vec{n}_{ij}$  is the outward unit normal associated with the face between nodes  $i$  and  $j$ ,  $\vec{u}_{\Omega_{ij}} = (\vec{u}_{\Omega_i} + \vec{u}_{\Omega_j})/2$  is the grid velocity at the dual cell face as an average of the grid velocities at nodes  $i$  and  $j$ ,  $U_i$  is the vector of conserved variables at point  $i$  and  $\vec{F}_i^c$  is the convective flux at node  $i$ .  $P$  is the matrix of eigenvectors of the convective flux Jacobian matrix  $\vec{A}^c$  constructed using the Roe-average variables and projected in the  $\vec{n}_{ij}$  direction and  $|\Lambda|$  is a diagonal matrix with entries corresponding to the absolute of the eigenvalues of the flux Jacobian matrix. The final term in Eq. 32 is the adjustment required for the convective flux due to motion of the domain when expressing the equations in ALE form.

## C. Roe Schemes for Hybrid RANS/LES

In this section, adaptations of the Roe scheme for Hybrid RANS/LES simulations are presented. The subsequent modifications are based on the coefficient  $\gamma$  used to control the amount of dissipation in the Roe scheme as

$$\tilde{F}_{ij}^c = \left( \frac{\vec{F}_i^c + \vec{F}_j^c}{2} \right) \cdot \vec{n}_{ij} - \sigma \left\{ \frac{1}{2} P |\Lambda| P^{-1} (U_i - U_j) \right\} - (\vec{u}_{\Omega_{ij}} \cdot \vec{n}_{ij}) \left( \frac{U_i + U_j}{2} \right) \quad (33)$$

with  $\sigma = 0$  being an almost central difference scheme and  $\sigma = 1$  being the unaltered scheme.

### 1. Winkler's Modification

Winkler et al.<sup>39</sup> proposed a coefficient which is based on Eq.34, a parameter  $f_d$  already available in DDES. The Winkler's modification is defined as

$$\sigma = \sigma_{FD} = \max(0.05, 1 - f_d). \quad (34)$$

As in DDES, the  $f_d$  parameter provides a blending from RANS to LES, somewhat protecting the boundary-layer from the reduced dissipation. The term  $\sigma$  is then prevented from becoming too small (in LES regions) and thus leading to potentially unstable solutions.

According to Winkler et al.,<sup>39</sup> the reduction of the Roe dissipation is only done for the momentum equations, the conservation of mass and energy are not altered from the original Roe scheme.

### 2. Travin's Hybrid Modification

Travin et al.<sup>40</sup> proposed a central/upwind hybrid inviscid scheme, originally designed to combine a central (fourth-order) and upwind (third- or fifth-order) approximation of inviscid flux in a structured high-order code. The modified blending function is given as

$$\sigma = \sigma_{NTS} = \sigma_{max} \tanh(A^{ch1}), \quad (35)$$

where

$$A = ch2 \max((C_{DES}\Delta/L_{turb}/g - 0.5), 0), \quad (36)$$

$$L_{turb} = \left[ \frac{\nu_t + \nu}{C_\mu^{3/2} K} \right]^{0.5}, \quad (37)$$

$$K = \max \left( \left[ \frac{\tilde{S}^2 + \Omega^2}{2} \right]^{0.5}, 0.1\tau^{-1} \right), \quad (38)$$

$$\tau = L_{nond}/U_\infty, \quad (39)$$

$$g = \tanh(B^4), \quad (40)$$

$$B = \frac{ch3 \Omega \max(\Omega, \tilde{S})}{\max \left( \frac{\tilde{S}^2 + \Omega^2}{2}, 10^{-20} \right)}. \quad (41)$$

The constants are given as:  $\sigma_{max} = 1$ ,  $ch1 = 3$ ,  $ch2 = 1$ ,  $ch3 = 2$  and  $C_{DES}$  is DES constant.

This function  $\sigma_{NTS}$  becomes its maximum value of 1.0 near the wall and in irrotational regions of the flow to guarantee instability of the scheme in coarse regions.<sup>41</sup> It is close to zero in the LES region, resulting in an “almost central” scheme to resolve turbulence structures.

#### D. Jameson-Schmidt-Turkel Scheme

The JST scheme<sup>30</sup> is a central difference method that controls numerical oscillations in the vicinity of shocks by adding a blend of two types of artificial dissipation. Both levels of dissipations are combined based on a pressure switch for triggering lower-dissipation on shock locations resulting a second-order scheme in space with flux approximated as (including the last term related to grid motion):

$$\tilde{F}_{ij}^c = \vec{F}^c \left( \frac{U_i + U_j}{2} \right) \cdot \vec{n}_{ij} - d_{ij} - (\vec{u}_{\Omega_{ij}} \cdot \vec{n}_{ij}) \left( \frac{U_i + U_j}{2} \right). \quad (42)$$

The artificial dissipation is expressed as

$$d_{ij} = \left( \epsilon_{ij}^{(2)}(U_j - U_i) - \epsilon_{ij}^{(4)}(\nabla^2 U_j - \nabla^2 U_i) \right) \varphi_{ij} \lambda_{ij}, \quad (43)$$

with the undivided Laplacians  $\nabla^2 U$ , local spectral radius, grid stretching and pressure switches computed as:

$$\nabla^2 U_i = \sum_{k \in N(i)} (U_k - U_i), \quad (44)$$

$$\lambda_{ij} = (|\vec{u}_{ij} - \vec{u}_{\Omega_{ij}} \cdot \vec{n}_{ij}| + c_{ij}) \Delta S, \quad \lambda_i = \sum_{k \in N(i)} \lambda_{ik}, \quad (45)$$

$$\varphi_{ij} = 4 \frac{\varphi_i \varphi_j}{\varphi_i + \varphi_j}, \quad \varphi_i = \left( \frac{\lambda_i}{4 \lambda_{ij}} \right)^\alpha, \quad (46)$$

$$\epsilon_{ij}^{(2)} = k^{(3)} s_2 \left( \frac{\left| \sum_{k \in N(i)} (p_k - p_i) \right|}{\sum_{k \in N(i)} (p_k + p_i)} \right), \quad \epsilon_{ij}^{(4)} = s_4 \max(0, k^{(4)} - \epsilon_{ij}^{(2)}), \quad (47)$$

where  $N(i)$  are the neighboring points,  $p_i$  the pressure,  $s_2$  and  $s_4$  stretching parameters and  $\alpha = 0.3$ ,  $\epsilon^{(2)} = 0.5$  and  $\epsilon^{(4)} = 0.02$  are typically used for unstructured meshes.

## V. Results

### A. Spatial Shear Layer

The objective of this numerical study is to assess the capability of different hybrid sub-grid length scales to simulate a spatially developing shear layer and mitigate the effect of the delay in the formation of 3D instabilities. An important issue in any Hybrid RANS/LES method is development of free shear layers

starting from incoming turbulent boundary layers treated in RANS mode. The free shear layer, intended to be treated in LES mode, may suffer from a delay in the formation of 3D instabilities due to the convection of eddy viscosity from the boundary-layer treated in RANS mode.<sup>16</sup>

The free flow studied here is generated at the trailing edge of a flat plate with free-stream velocities  $U_{high} = 41.54m/s$  and  $U_{low} = 22.4m/s$  at the different sides of the flat plate. The flow conditions correspond to the experiment of Delville,<sup>42</sup> the boundary layers are turbulent with momentum and displacement thickness equal to  $\theta_{high} = 1mm$  and  $\delta_{high}^* = 1.4mm$  at the high-speed side and  $\theta_{high} = 0.73mm$  and  $\delta_{high}^* = 1.0mm$  at the low-speed side. The Reynolds number based on the momentum thickness at the high-speed side is  $Re_{\theta_{high}} = 2900$ .

The computational domain has a section of  $2.0 \times 0.3m$  in the  $XY$  plane and  $0.15m$  in the spanwise direction. In order to capture the correct boundary-layer profiles at the trailing edge, the flat plate has a length of  $0.82m$  on the high-speed side and  $0.46m$  on the low-speed side. A computational test section is defined with a length of  $1m$  after the trailing edge with uniform grid in the streamwise and spanwise directions, followed by a buffer zone of  $1m$  length with a stretched grid. The grid has a uniform distribution of 48 and 320 points in the spanwise and streamwise directions of the computational test section, respectively. The total amount of grid points is approximately 3 millions.

This flow has been studied with the use of hybrid RANS/LES approaches, both zonal (Deck<sup>16</sup>) and non-zonal (Kok and van der Ven<sup>43</sup> and Shur et al.<sup>17</sup>). The chosen convective scheme is the JST with a small forth order dissipation coefficient to prevent odd-even oscillations ( $k^{(4)} = 10^{-4}$ ). The time-step is set to  $\Delta t = 10^{-6}s$  and 5 inner iterations in the dual-time stepping approach.

The table 1 presents the performed calculations, the implicit LES simulation (Case 1) is taken as the reference and is obtained by switching off the eddy viscosity at the trailing edge of the flat plate. Cases 2-4 correspond to different subgrid length-scale definitions.

**Table 1:** Definition of the calculations for the spatially developing shear layer.

Case	1	2	3	4
Method	ILES	DDES	DDES	DDES
Hybrid SGS	None for $x > T.E.$	$\Delta_{max}$	$\Delta_\omega$	$\Delta_{SLA}$

An overview of the turbulence content in the shear layer is presented in Figs. 1 and 2 showing, respectively, instantaneous iso-surface of the Q criterion contoured by the normalized vorticity magnitude and contours of the vorticity magnitude in the  $Z = 0$  plane.

In the reference implicit LES calculation (Case 1), instabilities in the shear layer are very close to the trailing edge and becomes three-dimensional immediately (Fig.1a). For the standard DDES calculation (Case 2), the development of the shear layer is strongly delayed (Fig.1b). The solution displays the behavior of a laminar shear layer: growth of two-dimensional Kelvin-Helmontz instability followed by a vortex pairing. The delayed in the formation of instabilities is impressive and the shear layer never becomes three-dimensional in the computational domain.

A dramatic improvement is achieved using the vorticity-based (Case 3) length scale (Fig.1c). Although there is a small delay compared to the implicit LES. The initial spanwise vortices appear closer to the trailing edge and show three-dimensional disturbances.

Further improvement is obtained with the shear layer adapted length scale (Case 4). The initial spanwise vortices start even closer to the trailing edge and finer turbulent structures are captured downstream (Fig.1d).

## B. Zero Pressure Gradient Flat Plate

As shown in the previous section, the modifications of the sub-grid length scale ensure a drastic acceleration of the transition from RANS to LES in free shear layer flow. However, for wall bounded flows these modifications need to shield the boundary layer from the so-called modeled stress depletion like the standard DDES which is known to exist in the original DES version.<sup>17</sup>

Based on the computations of a zero pressure gradient boundary layer (ZPGL) in a quasi-2D mode, i.e., assuming that the spanwise step of grid is extremely small (zero), resulting in  $\Delta_{max} = \max(\Delta x, \Delta y)$ , with the use of SA RANS model and SA-based DDES done by Spalart et. al.<sup>2</sup> on a fairly ambiguous grid (with a target value of the streamwise grid step equal to 10% of the initial boundary layer thickness), the values of the constants  $C_{d1}$  and  $C_{d2}$  involved in the  $r_d$  function (Eq. 18) have been set equal to 8 and 3,

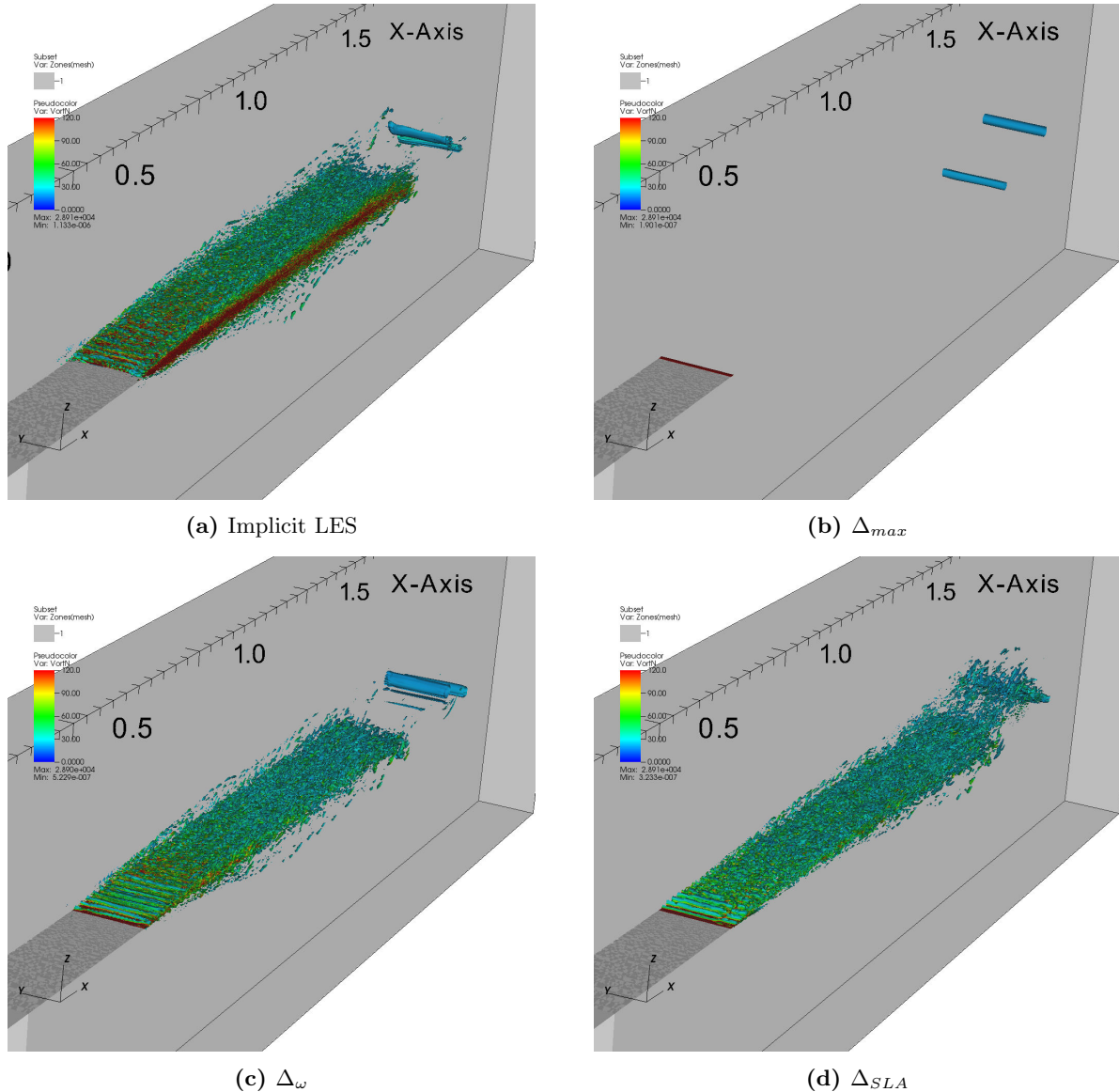


**Figure 1:** Iso-surface of Q criterion ( $Q = 100 * U_{high}/L$ ). Top (from left to right) Implicit LES, Standard DDES ( $\Delta_{max}$ ). Bottom (left to right) DDES with vorticity based SGS ( $\Delta_\omega$ ), DDES with Shear Layer Adapted SGS.

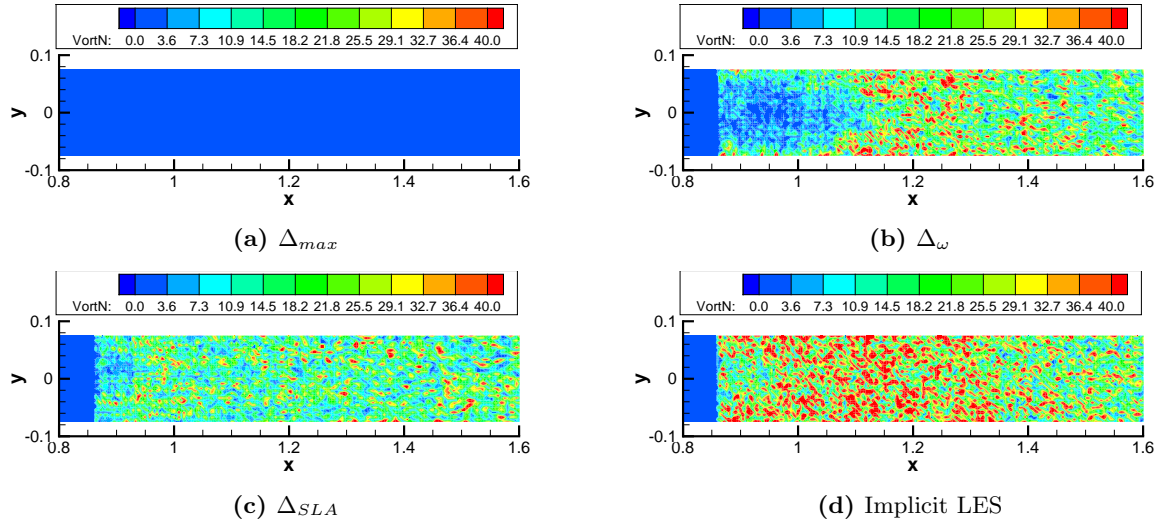


**Figure 2:** Contours of normalized vorticity magnitude at  $Z = 0$  plane. Top (from left to right) Implicit LES, Standard DDES ( $\Delta_{max}$ ). Bottom (left to right) DDES with vorticity based SGS ( $\Delta_\omega$ ), DDES with Shear Layer Adapted SGS.

respectively. Hence, in order to make sure that the vorticity-based ( $\Delta_\omega$ ) and the shear layer adapted  $\Delta_{SLA}$  length scales are compatible with DDES and preserve the shielding capability for wall-bounded flows with attached boundary layer regions, the  $f_d$  function should be evaluated and, if needed, some modifications should be proposed.

For the present ZPGL study, two grids of the NASA website ([https://turbmodels.larc.nasa.gov/flatplate\\_val.html](https://turbmodels.larc.nasa.gov/flatplate_val.html)) are used. The fine grid has  $545x385$  grid points while the coarse grid has  $137x97$  grid points, both grids have a  $y+ < 1$  over the flat plate. The reference Mach number is  $M_\infty = 0.2$  and the Reynolds number per unit length is  $Re = 5.10^6$ . Note that the boundary conditions for the DDES calculations are exactly the same of the RANS calculation, i.e., no turbulence is added at the inlet. A time-step of  $\Delta t = 0.01L/U_\infty$  was used in the DDES simulations.

Figure 3 presents the streamwise skin-friction coefficient over the flat plate for the coarse and fine grid. As expected for the coarse grid, the original DES version suffers from a strong modeled stress depletion while the standard DDES and the vorticity-based DDES present a correct skin-friction prediction compared to the RANS simulation. However, the shear layer adapted length scale shows a small deviation of the skin-friction coefficient near  $x = 0.5$  revealing that the  $F_{KH}^{lim}$  function was not enough to provide sufficient sheltering of the boundary layer. In contrast, both vorticity-based and shear layer adapted length scales present a premature switch to LES mode inside the boundary layer for the fine grid caused by a significant reduction of the eddy viscosity.

A simple way of eliminate this negative effect was proposed by Deck,<sup>16</sup> it takes advantage of the DDES function  $f_d$  to select the passage from  $\Delta = \Delta_{max}$  to  $\Delta = \Delta_\omega$  or  $\Delta = \Delta_{SLA}$ . This can be achieved by making  $\Delta$  sensitive to  $f_d$  with respect to a threshold value  $f_{d0}$  such as:

$$\Delta = \begin{cases} \Delta_{max} & \text{if } f_d < f_{d0} \\ \Delta_\omega \text{ or } \Delta_{SLA} & \text{if } f_d > f_{d0} \end{cases}$$

A significant improvement of the vorticity-based sub-grid length scale on the fine grid ensured by the use of the new  $f_{d0}$  constant is illustrated by Fig 4. The figure presents results of different  $f_{d0}$  values, it can seen that  $f_{d0} = 0.99$  is sufficient to provide the correct shielding of the boundary layer even on a fine grid.

### C. Backward Facing Step

The backward facing step (BFS) is a well documented and a mandatory case for any hybrid method. The desired behavior is to maintain RANS mode for the boundary layers on the upper and lower wall upstream

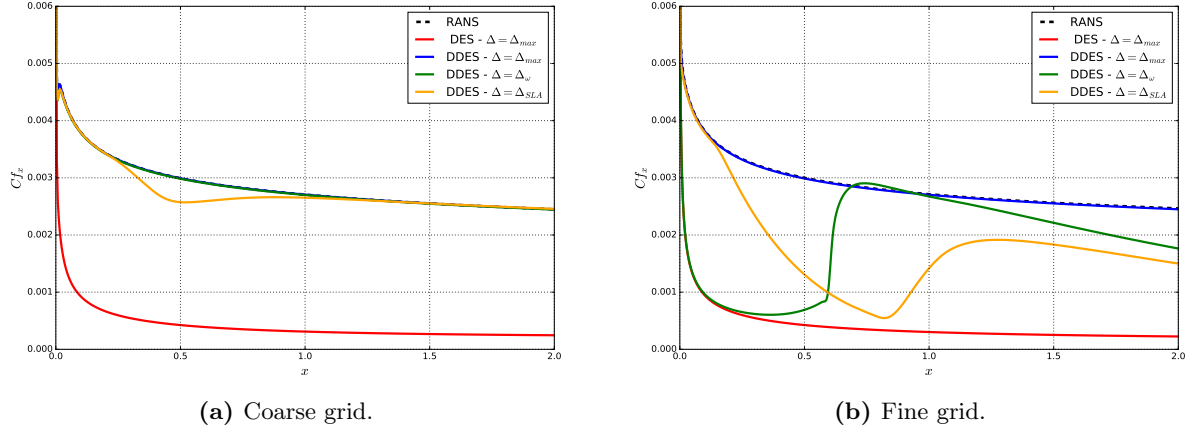


**Figure 3:** Distribution of streamwise skin-friction coefficient over the plate.

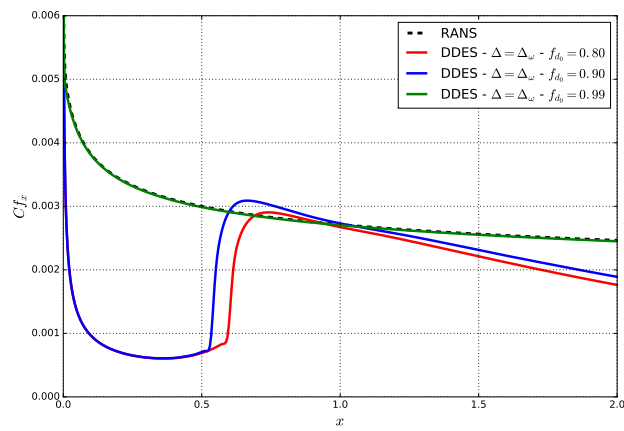


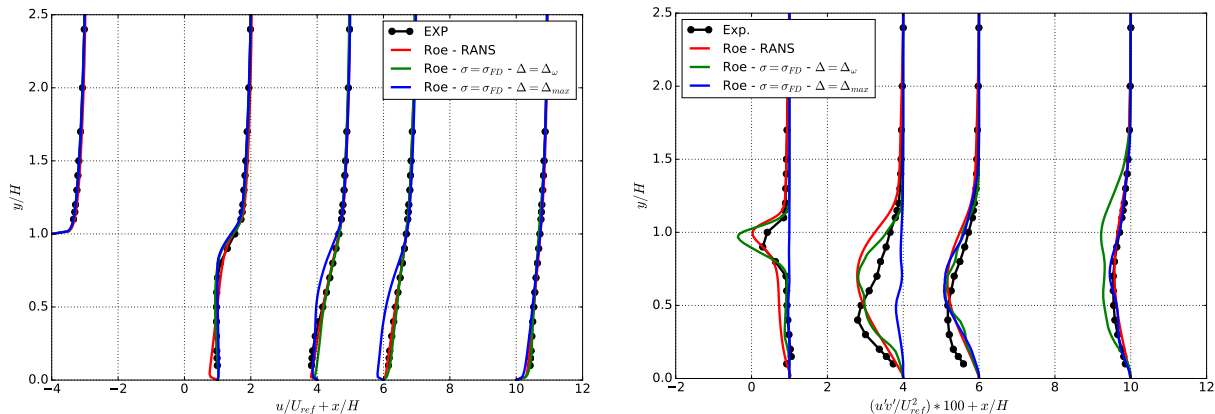
**Figure 4:** Comparison of the streamwise skin-friction distribution coefficient for different  $f_{d0}$  values.

of the step, located at  $x/h = 0$ . In this test case, we would like to study the capability of the vorticity-based length scale ( $\Delta_\omega$ ) to accelerate RANS/LES transition in the separated shear layer after the step. It is well known that the standard DDES ( $\Delta_{max}$ ) exhibits a considerable delay of transition from RANS to LES in the separated shear layer as demonstrated by Shur et al.<sup>17</sup> Thus, this flow is a representative test for checking if DDES combined with a modified sub-grid length scale ( $\Delta_\omega$  or  $\Delta_{SLA}$ ), provides the sheltering capability of the standard DDES ( $\Delta_{max}$ ) in the attached boundary layers, while achieves an acceleration of the RANS to LES transition in the separated shear layer, similar to what was observed in the spatial shear layer test case presented in a previous section.

The flow was studied experimentally by Driver and Seegmiller.<sup>44</sup> In this case, a turbulent boundary layer is developed and encounters a sudden back step. Then, the flow reattaches and recovers downstream of the step. The reference Mach number is  $M_\infty = 0.128$  and Reynolds number based on the step height is  $Re = 36000$ . A similar flow was computed with the use of the standard DDES and IDDES ( $\Delta = \Delta_{max}$ ) by Spalart et al.<sup>2</sup> and by Shur et al.,<sup>15</sup> respectively. In the context of the new sub-grid length scales proper for accelerate RANS/LES transition, this flow was computed with the use of Zonal DES by Deck<sup>16</sup> using the vorticity-based length scale ( $\Delta = \Delta_\omega$ ) and by Shur et al.<sup>17</sup> using the shear-layer adapted length scale ( $\Delta = \Delta_{SLA}$ ).

The two-dimensional grid (about 21000 grid points) of the NASA website ([https://turbmodels.larc.nasa.gov/backstep\\_val.html](https://turbmodels.larc.nasa.gov/backstep_val.html)) is used. This grid was extended in the spanwise direction with  $4h$  and a constant spanwise resolution of  $\Delta z/h = 0.1$ . The chosen convective scheme is the low-dissipation Roe based on the DDES  $f_d$  function (Eq.34). The time step is set to  $\Delta t = 0.02h/U_\infty$  with eighty inner iterations in the dual-time stepping approach. The total simulation time is  $30h/U_\infty$  where statistical average is performed over the last  $10h/U_\infty$ .

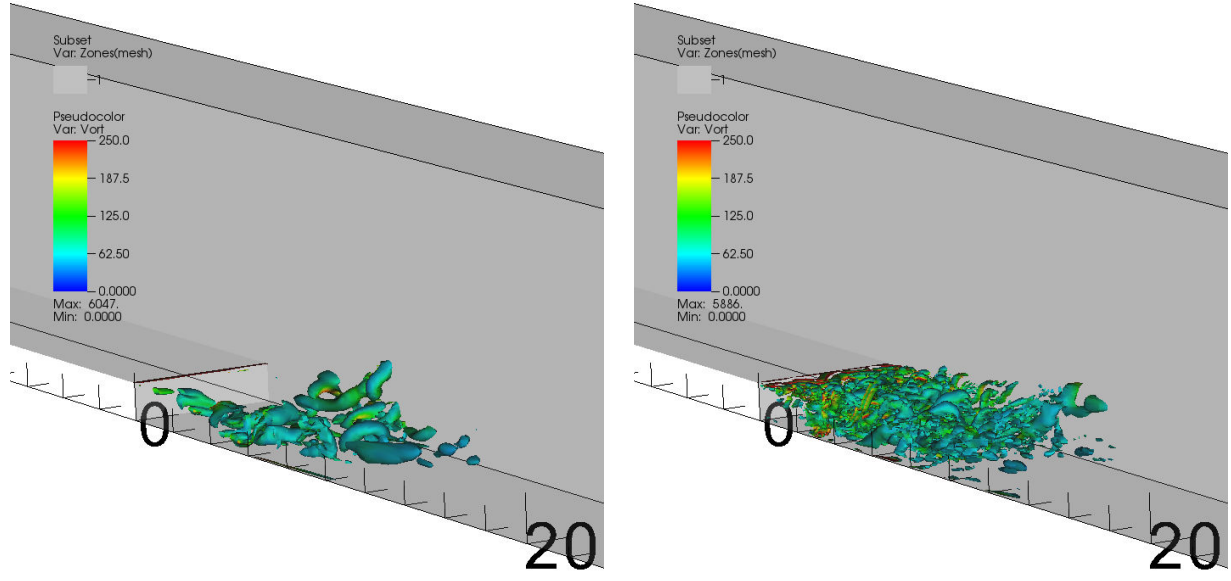
Figure 5 presents the mean streamwise velocity and Reynolds stresses profiles at different stations compared with the experiment using two different sub-grid length scales ( $\Delta = \Delta_{max}$  and  $\Delta = \Delta_\omega$ ), the RANS calculation is also presented for comparison. One can notice that the RANS treatment of the boundary layer is preserved at  $x/h = -4$  (upstream of the step) for both  $\Delta_{max}$  and  $\Delta_\omega$ . The main differences come from the treatment of the separated area, just after the step, in the LES mode. Indeed, the high levels of eddy viscosity coming from the attached boundary layer are convected to the LES region within the standard DDES. On the other hand, the vorticity-based length scale switches more rapidly to LES mode downstream of the separation point as highlighted by the accurate prediction of the Reynolds stresses fluctuations compared to the standard DDES.



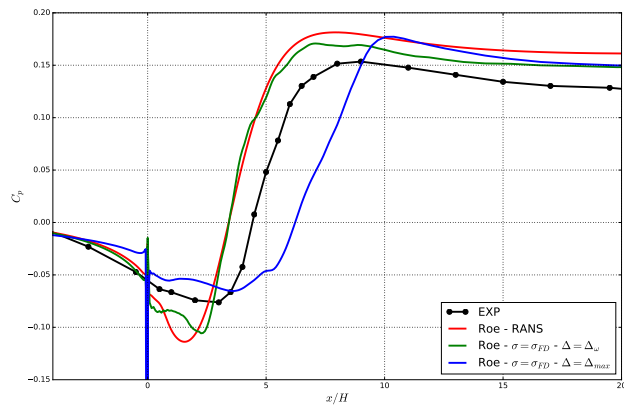
**Figure 5:** Mean streamwise velocity and Reynolds stresses profiles at different stations.

Figure 6 shows turbulent structures visualized by an iso-surface of Q-criterion. As already mentioned, it can be seen that these structures develop more quickly downstream of the step for the vorticity-based ( $\Delta = \Delta_\omega$ ) than the standard DDES ( $\Delta = \Delta_{max}$ ).

These observations are supported by the mean pressure coefficient distribution presented in Fig. 7. It shows that results of DDES combined with the length scale  $\Delta_\omega$  agree with experiment much better than the standard DDES ( $\Delta_{max}$ ) version. Deck<sup>16</sup> and Shur et al.<sup>17</sup> demonstrated the same improvement in the results using the vorticity-based ( $\Delta_\omega$ ) and shear layer adapted length scales ( $\Delta_{SLA}$ ), respectively, compared to the standard DDES.



**Figure 6:** Iso-surface of Q criterion ( $Q = 0.5 * U_\infty^2 / L^2$ ). Left, Standard DDES ( $\Delta_{max}$ ). Right, DDES with vorticity based SGS ( $\Delta_\omega$ ).



**Figure 7:** Mean streamwise velocity and Reynolds stresses profiles at different stations.

## D. NACA0021 Airfoil at Deep Stall

The high Reynolds number flow around airfoils at large (beyond stall) angles of attack is a challenging CFD problem of significant importance for the aerospace industry. The NACA0021 at sixty degrees angle of attack was chosen due to its well-documented behavior and numerous validation efforts for the implementation of Hybrid RANS-LES solutions in many CFD solvers.<sup>39,45–47</sup> The unsteady lift and drag time history and surface pressure coefficient were obtained in experiments conducted by Swalwell et al.<sup>48</sup> Hence, this flow seems to be a perfect test case for highlight differences of the above mentioned sub-grid length scales and also to evaluate the benefits of use a low-dissipation Roe scheme, given in Eq. 34.

The computational grid has an O-grid topology with a spanwise extent of  $1c$ . The grid has approximately  $4.0 \cdot 10^5$  cells with  $N_r = 82$ ,  $N_\theta = 162$  and  $N_z = 30$ , where  $N_r$ ,  $N_\theta$  and  $N_z$  denote the cell numbers in the radial, circumferential and spanwise directions, respectively. The far-field domain is situated at a distance of  $20c$  from the airfoil. A 2D dimensional view is presented in Fig.8. The surface of the airfoil is treated as a no-slip wall boundary, and the grid resolution is sufficient for full resolution to  $y+ = 1$  everywhere. As pointed out by Garbaruk et al.,<sup>49</sup> this flow reveal a strong sensitive to the size of spanwise computational domain. According to recommendations of Garbaruk et al.,<sup>49</sup> a fine grid was created multiplying the above mentioned 2D grid by a factor of 2 and the spanwise size was set equal to  $4c$  with a constant step  $\Delta z$  equal to  $0.02c$ . The boundary conditions in the spanwise direction are periodic. For all computations, the numerical time step was set to  $0.025c/U_\infty$ .

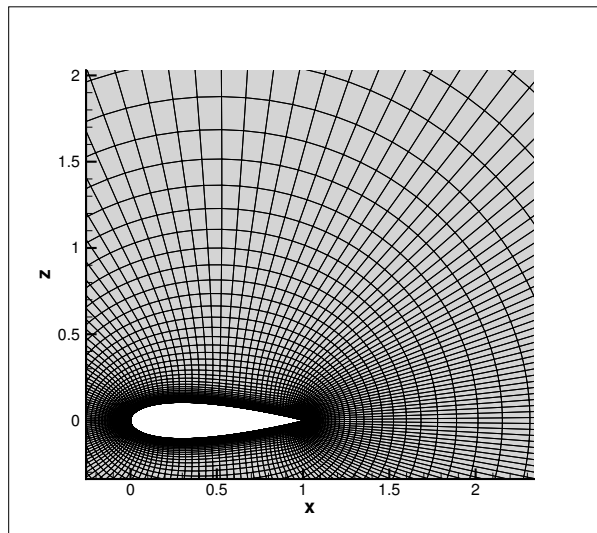


**Figure 8:** Near field view of the computational grid used for the NACA0021 test case.

Table 2 presents the performed calculations, the convective scheme Roe ( $\sigma = 1$ ) is the standard Roe scheme with dissipation coefficient equal to 1, the low-dissipation Roe ( $\sigma = \sigma_{FD}$ ) is based on the DDES  $f_d$  function acting as a standard Roe in RANS regions (boundary layers) with  $\sigma = 1$  and, as a low-dissipation scheme in LES regions with  $\sigma = 0.05$ .

**Table 2:** Definition of the calculations for the NACA 0021 airfoil at 60 degree of angle of attack.

Case	1	2	3	4	5
Method	URANS	DDES	DDES	DDES	DDES
Convective Scheme	Roe ( $\sigma = 1$ )	Roe ( $\sigma = 1$ )	Roe ( $\sigma = \sigma_{FD}$ )	Roe ( $\sigma = \sigma_{FD}$ )	Roe ( $\sigma = \sigma_{FD}$ )
Hybrid SGS	None	$\Delta_{max}$	$\Delta_{max}$	$\Delta_\omega$	$\Delta_\omega$
Grid	Coarse	Coarse	Coarse	Coarse	Fine

A dramatic improvement in solution fidelity for Hybrid RANS/LES (SA-DDES) compared to URANS was first reported by Shur et al.<sup>45</sup> The benefits of the original DDES ( $\Delta = \Delta_{max}$ ) compared to URANS are presented in Fig. 9 which compare the instantaneous spanwise vorticity computed with the original Roe

scheme, Cases 2 and 1. The effect of low dissipation convective schemes on the original DDES is investigated comparing Fig. 9b (Case 2) with Fig. 9c (Case 3). The use of the original Roe scheme strongly dump the fine vortices in the wake, while, a low dissipation scheme was seen to resolve fine turbulent structures in the wake region.

Further improvement is achieved using the vorticity-based ( $\Delta = \Delta_\omega$ ), Case 4, the eddy viscosity returned by the modified  $\Delta_\omega$  turn out to be less than the predicted by the original DDES, leading to a higher acceleration of the roll-up of the separated shear layers and to a finer resolution of the turbulent eddies in the wake region. One can see a qualitatively similar behavior to that observed in the backward facing step (see Fig. 6).

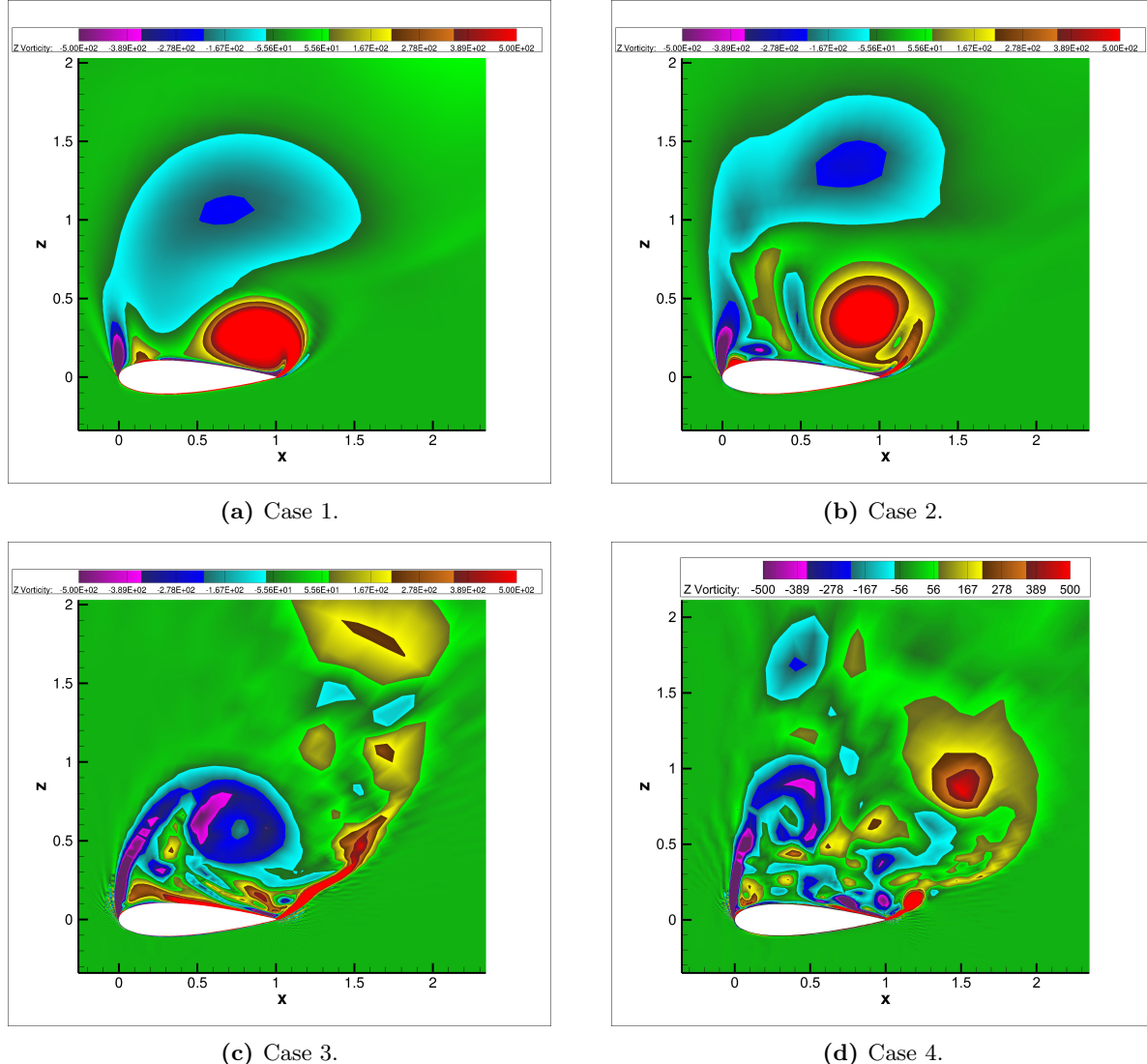


**Figure 9:** Contours of instantaneous spanwise vorticity computed with the original Roe scheme: RANS (left) and DDES(right).

Figure 10 presents a comparison of the power spectral density of the lift coefficient and the mean pressure distribution over the airfoil computed by Cases 1-4 using the coarse grid. For this particular coarse grid, all DDES simulations poorly predicted the main shedding frequency and failed to predict the harmonic of the shedding frequency. Whereas, the mean pressure distribution reveals a systematic difference between the predicted and measured pressure on the suction side. Although, Case 2 (standard Roe and original DDES) is close to the experiment, a concrete reason for the difference between low-dissipation and standard Roe predictions is not clear, in any case, it is not significant when compared to the differences between DDES

and URANS.

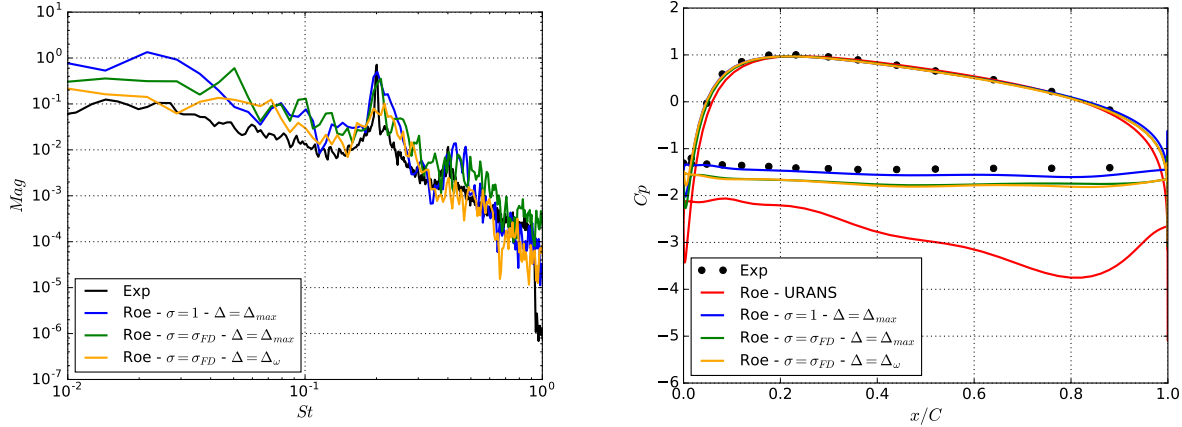


**Figure 10:** Comparison of PSD of lift coefficient and mean distribution of pressure coefficients predicted by Cases 1-4.

The effect of using a fine grid (Case 5) is demonstrated in Fig.11, where the PSD of the lift coefficient and the mean distribution of the pressure coefficient are compared with the coarse grid (Case 4) using the same vorticity-based DDES and low-dissipation scheme. One can note that the fine grid provides a most accurate PSD prediction where both main shedding frequency and its harmonic are correctly captured. Also, the mean pressure coefficient prediction is closer to the experimental data. Figure 12 illustrates the increase in the resolution of smaller and more intense turbulent eddies compared to the coarse grid and the presence of streamwise rib and spanwise von Kármán vortices in the wake region.

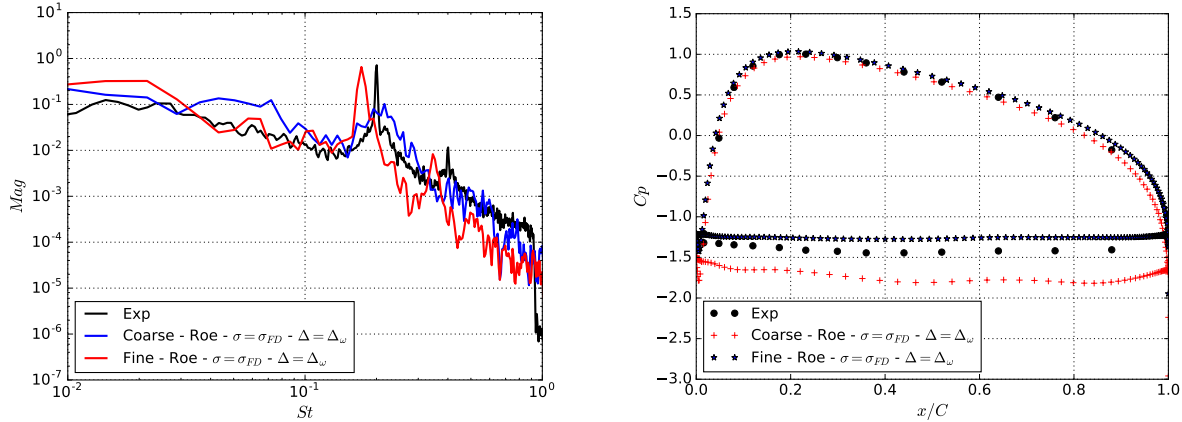


**Figure 11:** Comparison of PSD of lift coefficient and mean distribution of pressure coefficients predicted by the coarse and fine grid, Cases 4 and 5.

## VI. Conclusions

The Delayed Detached Eddy Simulation (DDES) approach was incorporated in SU2 and convincingly demonstrated its capabilities on a set of numerical examples including spatial shear layer, zero pressure gradient flat plate, backward facing step and NACA 0021 airfoil at deep stall. The implementation of DDES in SU2 was beyond the original DDES ( $\Delta = \Delta_{max}$ ), two sub-grid length scales, namely the vorticity-based ( $\Delta = \Delta_\omega$ ) and shear-layer adapted ( $\Delta = \Delta_{SLA}$ ) length scales, proper designed to “grey area” mitigation and faster RANS/LES transition were implemented and validated. Also, special attention was dedicated on the implementation of low-dissipation schemes proper for Hybrid RANS/LES simulations. Further work will be directed at the investigations of others industrial relevant test cases and the extension of the current

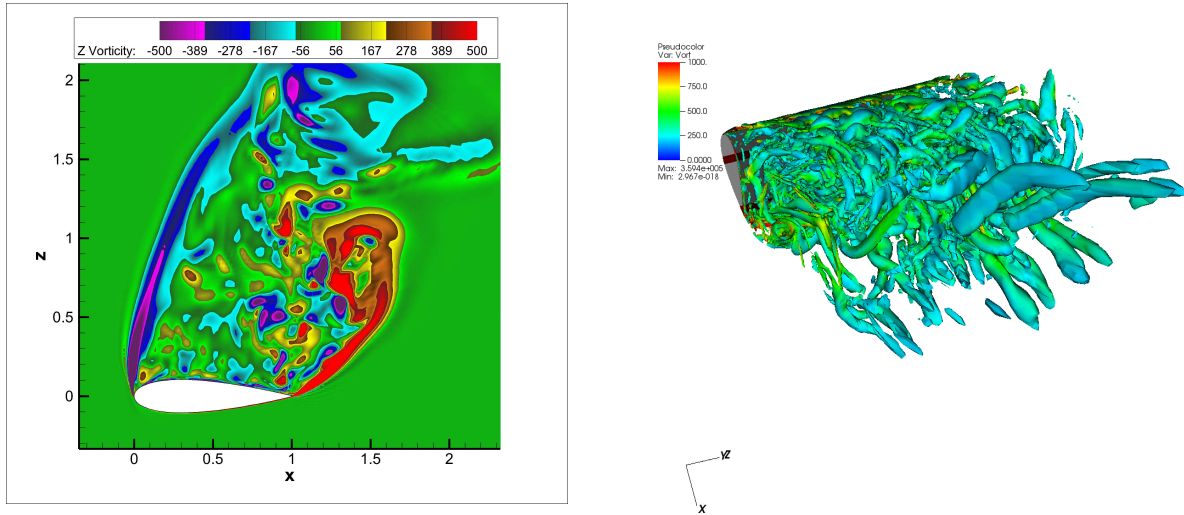


**Figure 12:** Contours of vorticity and Iso-surface of ( $Q = 0.1 * U_\infty^2 / L^2$ ) for the fine grid.

implementation to shock wave/boundary layer flows.

Lastly, SU2 is connected to a global community of researchers and developers and the present study can be used as a basis of future work and development of Hybrid RANS/LES methods.

## VII. Acknowledgements

The authors from ITA acknowledge the computational resources provided by ITA (grant FAPESP 2013/07375-0) and USP/Cepid-CeMEAI.

## References

- <sup>1</sup>Spalart, P., Jou, W., Strelets, M., Allmaras, S., et al., “Comments on the feasibility of LES for wings, and on a hybrid RANS/LES approach,” *Advances in DNS/LES*, Vol. 1, 1997, pp. 4–8.
- <sup>2</sup>Spalart, P., Deck, S., Shur, M., Squires, K., Strelets, M., and Travin, A., “A New Version of Detached-eddy Simulation, Resistant to Ambiguous Grid Densities,” *Theoretical and Computational Fluid Dynamics*, Vol. 20, No. 3, 2006, pp. 181–195.
- <sup>3</sup>Deck, S., “Zonal-detached-eddy simulation of the flow around a high-lift configuration,” *AIAA journal*, Vol. 43, No. 11, 2005, pp. 2372–2384.
- <sup>4</sup>Girimaji, S., Haase, W., Peng, S.-H., and Schwamborn, D., “Progress in Hybrid RANS-LES Modelling,” .
- <sup>5</sup>Peng, S.-H., Doerffer, P., and Haase, W., “Progress in Hybrid RANS-LES Modelling,” .
- <sup>6</sup>Fu, S., Haase, W., Peng, S.-H., and Schwamborn, D., “Progress in Hybrid RANS-LES Modelling,” .
- <sup>7</sup>Wilcox, D. C. et al., *Turbulence modeling for CFD*, Vol. 2, DCW industries La Canada, CA, 1998.
- <sup>8</sup>Sutherland, W., “The viscosity of gases and molecular force,” *Philosophical Magazine Series*, 1893.
- <sup>9</sup>Spalart, P. and Allmaras, S., “A one-equation turbulence model for aerodynamic flows.” *AIAA Paper 1992-0439*, 1992.
- <sup>10</sup>Tucker, P. G. and Tyacke, J. C., “Eddy resolving simulations in aerospace Invited paper (Numerical Fluid 2014),” *Applied Mathematics and Computation*, Vol. 272, Jan. 2016, pp. 582–592.
- <sup>11</sup>Spalart, P. R., “Detached-Eddy Simulation,” *Annual Review of Fluid Mechanics*, Vol. 41, No. 1, Jan. 2009, pp. 181–202.
- <sup>12</sup>Frhlich, J. and von Terzi, D., “Hybrid LES/RANS methods for the simulation of turbulent flows,” *Progress in Aerospace Sciences*, Vol. 44, No. 5, July 2008, pp. 349–377.
- <sup>13</sup>Menter, F. R. and Kuntz, M., “Adaptation of eddy-viscosity turbulence models to unsteady separated flow behind vehicles,” *The aerodynamics of heavy vehicles: trucks, buses, and trains*, Springer, 2004, pp. 339–352.
- <sup>14</sup>Ashton, N., “Recalibrating Detached-Eddy Simulation to eliminate modelled-stress depletion,” *23rd AIAA Computational Fluid Dynamics Conference*, American Institute of Aeronautics and Astronautics, 2017.
- <sup>15</sup>Shur, M. L., Spalart, P. R., Strelets, M. K., and Travin, A. K., “A hybrid RANS-LES approach with delayed-DES and wall-modelled LES capabilities,” *International Journal of Heat and Fluid Flow*, Vol. 29, No. 6, 2008, pp. 1638–1649.
- <sup>16</sup>Deck, S., “Recent improvements in the Zonal Detached Eddy Simulation (ZDES) formulation,” *Theoretical and Computational Fluid Dynamics*, Vol. 26, No. 6, Dec. 2012, pp. 523–550.
- <sup>17</sup>Shur, M. L., Spalart, P. R., Strelets, M. K., and Travin, A. K., “An Enhanced Version of DES with Rapid Transition from RANS to LES in Separated Flows,” *Flow, Turbulence and Combustion*, Vol. 95, No. 4, 2015, pp. 709–737.

- <sup>18</sup>Deck, S., "Numerical simulation of transonic buffet over a supercritical airfoil," *AIAA journal*, Vol. 43, No. 7, 2005, pp. 1556–1566.
- <sup>19</sup>Palacios, F., Colombo, M. R., Aranake, A. C., Campos, A., Copeland, S. R., Economou, T. D., Lonkar, A. K., Lukaczyk, T. W., Taylor, T. W., and Alonso, J. J., "Stanford University Unstructured (SU2): An open-source integrated computational environment for multi-physics simulation and design," *AIAA Paper*, Vol. 287, 2013, pp. 2013.
- <sup>20</sup>Palacios, F., Economou, T. D., Aranake, A. C., Copeland, S. R., Lonkar, A. K., Lukaczyk, T. W., Manosalvas, D. E., Naik, K. R., Padrón, A. S., Tracey, B., et al., "Stanford University Unstructured (SU2): Open-source analysis and design technology for turbulent flows," *AIAA paper*, Vol. 243, 2014, pp. 13–17.
- <sup>21</sup>Economou, T. D., Palacios, F., Copeland, S. R., Lukaczyk, T. W., and Alonso, J. J., "SU2: An Open-Source Suite for Multiphysics Simulation and Design," *AIAA Journal*, Vol. 54, No. 3, 2015, pp. 828–846.
- <sup>22</sup>Barth, T. J., "Aspect of unstructured grids and finite-volume solvers for the Euler and Navier-Stokes equations," *Lecture Notes Presented at the VKI Lecture Series*, 1994 - 05, Von Karman Institute for fluid dynamics, Rhode Saint Genese Begium, 2 1995.
- <sup>23</sup>Quarteroni, A. and Valli, A., *Numerical approximation of partial differential equations*, Vol. 23 of *Springer series in computational mathematics*, Springer-Verlag Berlin Heidelberg New York, 1997.
- <sup>24</sup>Jameson, A., "A perspective on computational algorithms for aerodynamic analysis and design," *Progress in Aerospace Sciences*, Vol. 37, 2001, pp. 197–243.
- <sup>25</sup>LeVeque, R., *Finite Volume Methods for Hyperbolic Problems*, Cambridge University Press, 2002.
- <sup>26</sup>Wesseling, P., *Principles of Computational Fluid Dynamics*, Vol. 29 of *Springer Series in Computational Mathematics*, Springer-Verlag Berlin Heidelberg New York, 2000.
- <sup>27</sup>Jameson, A., "Analysis and Design of Numerical Schemes for Gas Dynamics 1 Artificial Diffusion, Upwind Biasing, Limiters and Their Effect on Accuracy and Multigrid Convergence," *RIACS Technical Report 94.15, International Journal of Computational Fluid Dynamics*, Vol. 4, 1995, pp. 171–218.
- <sup>28</sup>Jameson, A., "Analysis and Design of Numerical Schemes for Gas Dynamics 2 Artificial Diffusion and Discrete Shock Structure," *RIACS Report No. 94.16, International Journal of Computational Fluid Dynamics*, Vol. 5, 1995, pp. 1–38.
- <sup>29</sup>Toro, E. F., *Riemann Solvers and Numerical Methods for Fluid Dynamics: a Practical Introduction*, Springer-Verlag, 1999.
- <sup>30</sup>Jameson, A., Schmidt, W., and Turkel, E., "Numerical solution of the Euler equations by finite volume methods using Runge-Kutta time stepping schemes," *AIAA Paper 1981-1259*, 1981.
- <sup>31</sup>Roe, P. L., "Approximate Riemann solvers, parameter vectors, and difference schemes," *Journal of computational physics*, Vol. 43, No. 2, 1981, pp. 357–372.
- <sup>32</sup>van Leer, B., "Towards the Ultimate Conservative Difference Scheme V. A Second-order Sequel to Godunov's Method," *Journal of Computational Physics*, Vol. 32, No. 1, July 1979, pp. 101–136.
- <sup>33</sup>Venkatakrishnan, V., "On the Accuracy of Limiters and Convergence to Steady State Solutions," *AIAA Paper 1993-0880*, 1993.
- <sup>34</sup>Blazek, J., *Computational Fluid Dynamics: Principles and Applications*, Elsevier, Oxford, 2005.
- <sup>35</sup>Eliasson, P., "EDGE, a Navier-Stokes solver for unstructured grids," Tech. Rep. FOI-R-0298-SE, FOI Scientific Report, 2002.
- <sup>36</sup>Saad, Y. and Schultz, M. H., "GMRES: A generalized minimal residual algorithm for solving nonsymmetric linear systems," *SIAM J. Sci. Stat. Comput.*, Vol. 7, 1986, pp. 856–869.
- <sup>37</sup>Jameson, A., "Time dependent calculations using multigrid, with applications to unsteady flows past airfoils and wings," *AIAA Paper 1991-1596*, 1991.
- <sup>38</sup>Jameson, A. and Schenectady, S., "An Assessment of Dual-Time Stepping, Time Spectral and Artificial Compressibility Based Numerical Algorithms for Unsteady Flow with Applications to Flapping Wings," *AIAA Paper 2009-4273*, 2009.
- <sup>39</sup>Winkler, C., Dorgan, A., and Mani, M., "A Reduced Dissipation Approach for Unsteady Flows on Unstructured Grids," *AIAA, American Institute of Aeronautics and Astronautics*, Jan. 2012.
- <sup>40</sup>Travin, A., Shur, M., Strelets, M. M., and Spalart, P. R., "Physical and numerical upgrades in the detached-eddy simulation of complex turbulent flows," *Advances in LES of complex flows*, Springer, 2002, pp. 239–254.
- <sup>41</sup>Xiao, Z., Liu, J., Huang, J., and Fu, S., "Numerical Dissipation Effects on Massive Separation Around Tandem Cylinders," *AIAA Journal*, Vol. 50, No. 5, May 2012, pp. 1119–1136.
- <sup>42</sup>Delville, J., *La décomposition orthogonale aux valeurs propres et l'analyse de l'organisation tridimensionnelle des écoulements turbulents cisailés libres*, Ph.D. thesis, University of Poitiers, 1995.
- <sup>43</sup>Kok, J. and van der Ven, H., "Destabilizing free shear layers in X-LES using a stochastic subgrid-scale model," *Progress in Hybrid RANS-LES Modelling*, Springer, 2010, pp. 179–189.
- <sup>44</sup>Driver, D. M. and Seegmiller, H. L., "Features of a reattaching turbulent shear layer in divergent channelflow," *AIAA journal*, Vol. 23, No. 2, 1985, pp. 163–171.
- <sup>45</sup>Shur, M., Spalart, P., Strelets, M., and Travin, A., "Detached-eddy simulation of an airfoil at high angle of attack," *Engineering turbulence modelling and experiments*, Vol. 4, 1999, pp. 669–678.
- <sup>46</sup>Mockett, C., *A Comprehensive Study of Detached Eddy Simulation*, Univerlagtuberlin, 2009.
- <sup>47</sup>Guseva, E. K., Garbaruk, A. V., and Strelets, M. K., "Assessment of Delayed DES and Improved Delayed DES Combined with a Shear-Layer-Adapted Subgrid Length-Scale in Separated Flows," *Flow, Turbulence and Combustion*, 2016, pp. 1–22.
- <sup>48</sup>Swalwell, K., Sheridan, J., and Melbourne, W., "Frequency analysis of surface pressures on an airfoil after stall," *AIAA Paper*, Vol. 3416, 2003, pp. 2003.
- <sup>49</sup>Garbaruk, A., Leicher, S., Mockett, C., Spalart, P., Strelets, M., and Thiele, F., "Evaluation of time sample and span size effects in DES of nominally 2D airfoils beyond stall," *Progress in Hybrid RANS-LES Modelling*, Springer, 2010, pp. 87–99.